Power Quality Enhancement in Hybrid PV-BES System based on ANN-MPPT

HELİN BOZKURT

ÖZGÜR ÇELİK

AHMET TEKE

Power quality enhancement in hybrid PV-BES system based on ANN-MPPT

Helin BOZKURT[1,*] , **Özgür ÇELİK**[2] , **Ahmet TEKE**[3]

[1]Department of Electrical and Electronics Engineering, Faculty of Engineering,
Tarsus University, Mersin, Turkiye
[2]Department of Energy Systems Engineering, Faculty of Engineering,
Adana Alparslan Türkeş Science and Technology University, Adana, Turkiye
[3]Department of Electrical and Electronics Engineering, Faculty of Engineering,
Çukurova University, Adana, Turkiye

Abstract: Battery energy systems (BESs) assisted photovoltaic (PV) plants are among the popular hybrid power systems in terms of energy efficiency, energy management, uninterrupted power supply, grid-connected and off-grid availability. The primary objective of this study is to enhance the power quality of a grid-tied PV-BES hybrid system by developing an operational strategy based on artificial neural network (ANN) based maximum power point tracking (MPPT) method. A test system comprising a 10-kWh BES and a 12.4 kW PV plant is structured and simulated on the MATLAB/Simulink platform. The hybrid system is validated with three different cases: constant radiation, rapid changing radiation, and real-day solar radiation data from the Turkish State Meteorological Service of Tarsus (Mersin, Türkiye) employing the developed operational strategy. These cases involve the examination of three distinct MPPT methods, analyzing DC-link voltage, battery state of charge (SOC), current, voltage, and system total harmonic distortion (THD). The simulation results indicate that the developed operational strategy with the ANN-MPPT method yields superior THD results in output current and a more stable DC-link voltage. Furthermore, the strategy shows improved convergence speed and reduced oscillations to achieve diverse reference operating points under varying atmospheric conditions compared to conventional MPPT methods. Numerical results demonstrate that the developed operational strategy with the ANN-MPPT consistently maintains THD values below 3% and exhibits a stable DC-link voltage deviation of 1.42% in various charging modes for both rapidly changing radiation and real-day solar radiation data.

Key words: Battery energy storage system (BESs), total harmonic distortion (THD), ANN-based MPPT, grid connected hybrid systems, power quality enhancement

1. Introduction

Nowadays, the interest in renewable energy sources (RESs) has gradually increased on account of the exhaustion of traditional energy sources, their harm to nature, and the inability to meet sufficient energy demand. Solar power stands out as an extremely effective renewable energy source for various reasons, including its sustainability, cost-effectiveness, lack of pollution, and ease of installation [1]. With the increasing connection of RESs and other distributed generation (DG) units to utility power grids, the decline in power quality at the point of common coupling (PCC) has emerged as a notable concern [2]. Solar cells transform sunlight into electrical energy through the photoelectric effect. PV systems, comprised of semiconductor devices known as

---

*Correspondence: helinbozkurt@tarsus.edu.tr

photovoltaic modules, directly convert the sun's radiation into usable electricity. The output of PV power is significantly influenced by solar irradiation and temperature [3]. Consequently, optimizing the extraction of maximum power from the PV system is crucial for increasing the efficiency of solar power generation under various weather conditions. Therefore, the implementation of a suitable maximum power point tracking (MPPT) technique to precisely follow the maximum power point (MPP) is imperative. As a result, there is a significant demand for a suitable technique to accurately track the MPPT [4]. Since the produced power of the PV panel is directly dependent on the weather conditions, the behavior of the generated PV power is discontinuous. Thus, it is not always possible for the PV array to meet the load demand independently at all times [5]. This causes power mismatch and imbalance in the system. In order to minimize these problems occurring in the system and to increase the efficient use of energy, BESs are used with PV systems. BESs have several merits compared to conventional energy sources, such as prompt and stable responsiveness, adaptability, controllability, and independence from geographical limitations. Additionally, they are assessed as a potential solution to the challenges posed by the global warming problem [6]. As a significant contributor to clean energy, PV systems have experienced a recent surge in utilization, leveraging abundant and freely available solar energy. Nevertheless, when compared to other renewable technologies, PV systems encounter challenges such as high costs and low efficiency. Furthermore, the intermittent nature of solar energy introduces disturbances in the generated power, resulting in unfavorable system behavior. A high share of PV plants in the energy mix may induce power quality issues such as frequency variations, total harmonic distortion (THD) [7], voltage variations, and transient disturbances across power networks. Inadequate power quality management can lead to energy losses, equipment malfunctions, and grid instability. The choice of converter topology affects how effectively the system can handle varying environmental conditions and load demands, impacting overall system efficiency and reliability. Effective power management algorithms and controllers are essential for optimizing energy conversion efficiency and ensuring stable operation under dynamic conditions, including partial shading and varying solar irradiance. Addressing these power quality issues through proper design, integration, and control strategies is essential for maximizing the economic and environmental benefits of PV systems while maintaining grid stability and reliability. These factors collectively contribute to enhancing the overall performance and longevity of PV installations in diverse operational environments. Various studies in the literature have explored power quality issues associated with different methods and system topologies, as summarized in Table 1.

Table 1. Summary of power quality issues across different methods and system topologies.

Ref.	Year	Method	System type	Contribution
[8]	2017	An ANN-based hybrid MPPT method	Grid-tied PV system	The results demonstrate that the ANN-based hybrid MPPT model excels in terms of convergence speed. Additionally, the number of steady-state oscillations is minimized, and the confusion in perturbation direction is resolved.
[9]	2018	An adaptive deloading scheme with Lagrange interpolating polynomial technique	Wind turbine generator (WTG)	Validated through hardware-in-the-loop (HIL) simulations and accounting for wake effects, the approach enhances system frequency dynamics, wind farm efficiency, frequency stability, offering smoother dynamics and quicker settling times compared to traditional methods.
[10]	2018	An enhanced power management control approach	DC microgrid (MG) system PV, WTC, BES, fuel cell, and electrolyser	The simulation results are presented for various cases. Adaptive TS-fuzzy PI-controller tuning improves DC MG voltage response. Inverter-side proportional gain control ensures stability across varying conditions, including wind speed changes, load fluctuations, and islanding mode, while priority-based load shedding balances power among energy sources and storage during islanding.

Continued on next page

Ref.	Year	Method	System type	Contribution
[11]	2018	A fuzzy space vector pulse width modulation (FSVPWM) controller with hybrid fuzzy particle swarm optimization MPPT	Grid-tied hybrid PV-wind system	The study demonstrates the performance of FPSO MPPT and FSVPWM algorithms under varying conditions, providing enhanced system efficiency, reduced harmonics, and effective control, validated through experimental results on the dSPACE platform.
[12]	2019	An intelligent fuzzy particle swarm optimization (FPSO) MPPT with modified space vector pulse width modulation (SVPWM) controller	Grid-tied PV system	Both simulation and experimental results demonstrate that the hybrid FPSO MPPT and modified SVPWM-based controller operates without steady-state error and delivers rapid and accurate tracking for varying irradiance levels, eliminating oscillations around the MPP compared to conventional controllers.
[13]	2020	A modified demagnetization control strategy	Grid-tied WT system	Integrating external resistance on the stator accelerates the damping of transient flux by reducing the time constant. The demagnetization control strategy significantly improves transient responses—such as rotor current, stator current, electromagnetic torque, and DC-link voltage—during both symmetrical and asymmetrical grid faults.
[14]	2020	A passivity-based control scheme	Grid-tied PV system	The study presents a PBC scheme for inverters, showing through simulation and experimental results that it enhances power quality in grid-connected PV systems by reducing THD, improving PF, and managing various power types under nonlinear loads, all while reducing system cost, size, and weight.
[15]	2021	Current reference control MPPT with power management algorithm	Grid-tied hybrid PV-BES System	The results demonstrate through detailed experiments across various cases and performance comparisons with different control techniques that the proposed method achieves nearly 99% MPP tracking efficiency, rapid DC-link voltage regulation, low harmonic distortion, and optimal power quality, even under partial shading and transient conditions.
[16]	2021	A hybrid shuffled frog leaping and pattern search (HSFL–PS) algorithm based ANN-MPPT	Grid-tied hybrid PV-BES system	The performance of the hybrid ANN-MPPT is evaluated against several key conventional and intelligent MPPT algorithms. The graphical results show that the hybrid ANN-MPPT demonstrates the best performance.
[17]	2022	A new continuous mixed p-norm (CMPN) based adaptive asymmetrical fuzzy logic controller (AAFLC) method as inverter controller	Grid-tied PV system	The graphical results of the system are presented for various scenarios and supported with experimental results. The system exhibits low THD in grid voltage and inverter current.
[18]	2022	An adaptive TS-fuzzy based RBF neural network based MPPT	Grid-tied PV system	The study's experimental setup confirms that the evolved MPPT controller outperforms TS-fuzzy and GA-RBF neural network-based controllers, showing superior recognition speed, enhanced robustness, and optimal PV power tracking for changing sun insolation levels.
[19]	2022	A hybrid simplified firefly and neighborhood attraction firefly (HSFNA) algorithm based MPPT with the proposed high-gain step-up SEPIC converter	Hybrid PV fed battery system	The integrated HSFNA-based MPPT tracker and SEPIC converter offer accurate response, low energy loss, high efficiency, fast convergence, stability without oscillations tracking under varying solar conditions. These outcomes are validated through comprehensive simulation and experimental testing.
[20]	2022	A hybrid fuzzy-sliding mode MPPT with unified power quality conditioners	Hybrid PV-BES system	The proposed system is evaluated under various scenarios, and the simulation results demonstrate minimized THD, improved power factor towards unity, and reduced settling time.
[21]	2023	A nonlinear control strategy with energy management strategy with ANN-MPPT	Grid-tied hybrid PV-BES System	The simulation results for several cases are presented in the paper. This paper introduces an energy management system that creates multiple energy flow scenarios to balance energy distribution between the load and various sources.
[22]	2023	A novel multimode control strategy	Grid-tied hybrid PV-Wind-BES system	The proposed controller effectively manages grid-connected and islanding modes, enhancing power quality, mode transfer capabilities, and system robustness, while reducing current THD, as validated via simulation results.
[23]	2024	A novel Z-source DC-DC converter with ANFIS-PSO MPPT	Grid-tied PV system	The study experimentally validates a high gain Z-network DC-DC converter with an ANFIS-PSO-based MPPT algorithm, demonstrating efficient peak power extraction and enhanced grid power quality metrics including stable DC voltage, and reduced THD under various conditions.

Ref.	Year	Method		System type	Contribution
[24]	2024	Data-driven methods	MPPT	Hybrid (PV-FC-BES) DC MG	The operational strategy using various data-driven MPPT methods is analyzed for different cases, and a three-layer neural network-based MPPT technique is developed, significantly enhancing response time, efficiency, and accuracy in vehicular FC systems within DC hybrid microgrids. Additionally, a robust power-sharing strategy among FC, PV, and ESS units is introduced, ultimately improving system performance and sustainability.

The main purpose of this study is to increase the power quality of the PV-BES hybrid system using the developed operational strategy based on ANN-MPPT. The major contributions of this paper to the literature can be listed as follows:

- This study emphasizes the importance of uninterrupted, continuous, efficient use of energy, and a sample hybrid PV-BES system is modeled to promote the use of renewable energy, especially in low-power buildings.

- The study integrates the ANN-MPPT method with a hybrid PV-BES system, demonstrating its effectiveness under varying irradiance conditions.

- A unique operational strategy is developed and applied, addressing multiple operating modes such as charging, discharging, and PV to grid modes.

- The system's performance is validated using solar radiation data measured by the Turkish State Meteorological Service, enhancing the practical applicability of the results.

- The study provides a detailed comparative analysis of the ANN-MPPT method against conventional MPPT methods (P&O-MPPT and INC-MPPT) under three different radiation cases: constant, rapid changing, and real-day conditions.

- The results demonstrate that the ANN-MPPT method significantly improves system stability and power quality by reducing THD, ensuring a more stable DC-link voltage, and achieving quicker convergence to the MPP with less oscillation.

- The research presents an in-depth simulation analysis in MATLAB/Simulink, showcasing the performance improvements in terms of DC-link voltage stability and THD across different scenarios.

The paper is structured as follows: After the introduction, Section 2 details the hybrid energy system components, including the PV plant, BES system, DC-DC converter topologies, MPPT methods, and the developed operational strategy. Section 3 presents the results and discussions of the cases, while Section 4 concludes the study.

2. Hybrid energy conversion system

2.1. The proposed system overview

This study aims to reduce the current harmonic by developing an FFBPNN-based MPPT method, compared to the traditional-based perturb and observe (P&O) and incremental conductance (INC) MPPT methods, with the goal of optimizing the design for the grid-connected PV-BES system. The proposed system outline diagram is presented in Figure 1. The system is simulated using MATLAB/Simulink.
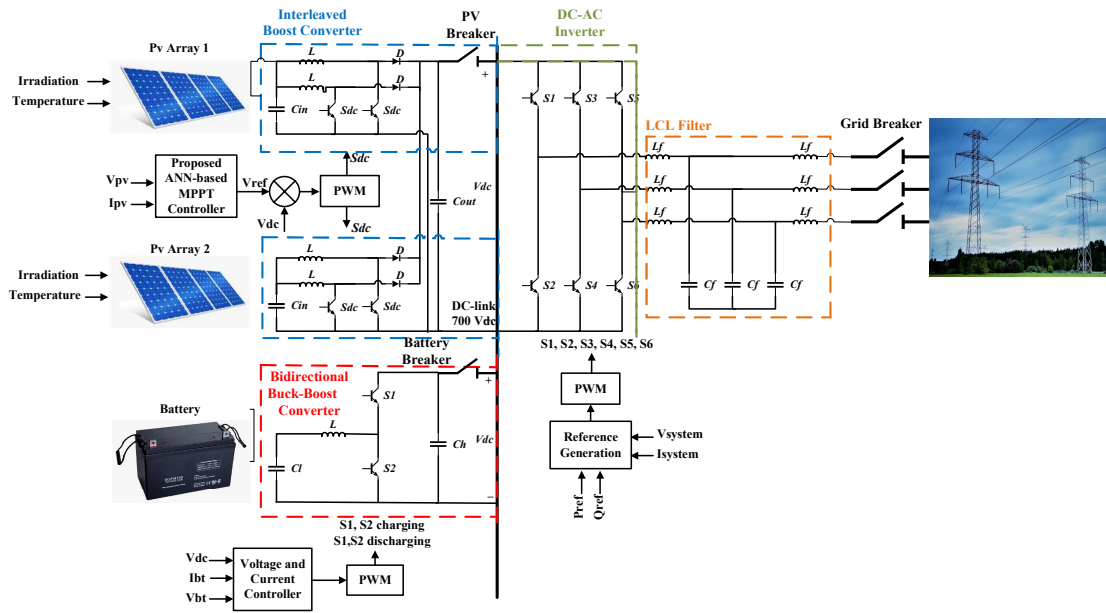
Figure 1. Overview of the proposed system [25].

2.2. Solar power

In this section, the design of the proposed system structure is explained in detail. The subsections cover the design of the PV array, the DC-DC interleaved boost converter, and both the conventional and the proposed ANN-based MPPT designs, respectively.

2.2.1. PV panel and characteristic

The solar power in the system is divided into two parts to account for potential shading scenarios. This approach aims to make the produced power more realistic, considering variable weather conditions. A solar power system with a total power of 12.48 kW is considered at two separate points, with the power divided equally. Thus, by creating two separate arrays, as specified in Table 2, the power of each array is determined to be 6.24 kW. These PV arrays are obtained by connecting two strings in parallel, with each string consisting of 12 serially connected modules. The output voltage, current, and power of the PV arrays are presented in Table 2 under standard test conditions (STC) for 1000 W/m^2 at 25 °C.

2.2.2. DC-DC interleaved boost converter design

Interleaved boost converters consist of two or more boost converters connected in parallel. The interleaved boost converter configuration enhances reliability and productivity while reducing the size of filter components. Additionally, it decreases ripple voltage and current compared to traditional boost converters [26]. The DC-DC interleaved boost converter topology is displayed in Figure 1. The design equations for the interleaved boost converter are as follows: V$_{PVmin}$ is the minimum voltage of the PV, V$_{DC-link}$ is the DC-link voltage, ΔI$_{in}$ is the change in the input current, and f$_{sw}$ is the switching frequency.

$$L \equiv \frac{V_{PVmin} * V_{DC-link} - V_{PVmin}}{f_{sw} * \Delta I_{in} * V_{DC-link}} \tag{1}$$

$$C \equiv \frac{I_{in} * V_{DC-link} - V_{PVmin}}{f_{sw} * \Delta V_{DC-link} * V_{DC-link}} \tag{2}$$

A two-layer DC-DC interleaved boost converter is designed to operate the PV system at the MPP. Two separate switches operate with a $180°$ phase shift under the control of the MPPT controller, functioning as two separate boost converters. By dividing the current into two branches, the transmission losses (I^2R) are reduced, leading to a more efficient operating system. The converter also reduces ripples in the output voltage and current. The interleaved boost converter consists of input and output capacitors, power switches, and inductors. Selecting the appropriate inductor and capacitor is crucial, as variations in the input and output waveforms affect controller performance, which in turn influences the overall system efficiency. The limit values for fluctuations in input current and output voltage are defined as 10% and 1%, respectively.

2.3. Controller design for power quality enhancement

2.3.1. P&O and INC methods

The P&O method is one of the simplest and most commonly used online MPPT techniques. This method observes the fluctuation in output power (dP) and subsequently identifies the direction of the operating voltage (dV). During the procedure, the reference voltage undergoes slight disturbances, and the system's response is carefully observed. This observation helps ascertain the direction for the subsequent perturbation [27]. The MPP position in the P&O method establishes the operation point's location in relation to the MPP, relying on the nonlinear characteristics of the solar array. It involves oscillating the operation point back and forth to attain the MPP by introducing perturbations in the PV voltage, current, or duty ratio [28]. The P&O-MPPT technique has certain drawbacks that notably impact the output power of the PV system. These include the size of the perturbation, which constrains the convergence rate and defines the amplitude of oscillations around the Vmpp. Another drawback is that this method induces power loss during perturbation and struggles to track the MPP under varying radiation and temperature conditions [29].

INC MPPT algorithm is widely adopted due to its simplicity in implementation. The INC technique tracks the MPP by considering the P-V characteristic of the PV module. It is based on the concept that the rate of change (derivative) of the output power (P) with respect to the panel voltage (V) is zero at the MPP [4]. The changes in voltage, current, and power define the direction of the perturbation. The INC method has many advantages including parameters such as tracking speed, accuracy, and efficiency. Despite these benefits, the INC algorithm encounters two primary challenges: continual oscillations persist even after achieving a steady state, and it demonstrates inefficiency in adapting to abrupt changes in operating conditions [30].

2.3.2. Proposed ANN-based MPPT controller

ANNs are computational models inspired by the human brain [31]. It is generally used for complex and nonlinear problems by regulating weights and biases [32]. ANN can be described as a parallel and distributed information processing framework that consists of input layers, at least one hidden layer, and an output layer. These layers are composed of interconnected neurons, the fundamental processing units [33]. The FFBPNN is a learning method that employs guidance and is used to establish the connection between input and output variables by adjusting the weights and biases to minimize the error. The basic structure of the FFBPNN model is illustrated in Figure 2. It consists of an input layer, an output layer, and at least one hidden layer.
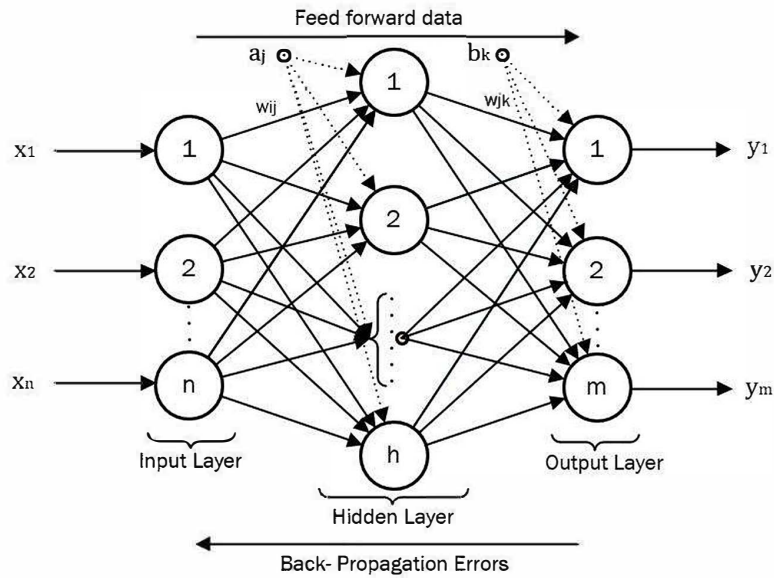
Figure 2. FFBPNN structure [34].

The model parameters of the FFBPNN in Figure 2 are outlined as follows; $x_1, x_2, .., x_n$ represent the inputs, $y_1, y_2, .., y_m$ denote the outputs. The computation of the output of the hidden layer, denoted as h_j, is determined as follows [35]:

$$h_j \equiv f\left(\sum_{i=1}^{n} w_{ij} - \alpha_i\right) \quad \text{j=1,2,..h,} \tag{3}$$

where f is the activation function of neurons, h is the total neuron number in hidden layers, n is the total neuron number in the input layer, w_{ij} is the weight of ith neuron on jth hidden neuron, and a_i is the bias value hidden neuron.

The ANN method reduces the continuous oscillations at the MPP during dynamic irradiation conditions [29]. The utilization of ANN-based MPPT has been demonstrated to possess the capability to efficiently track the MPP with minimal transient time and low ripple under actual operational climatic conditions. However, an accurate, standardized, and appropriate training dataset is the main limitation for optimal performance of ANN without high training error [36]. The objective of developing an AI-based controller is to deliver a more prompt response to changing weather conditions, ensuring uninterrupted system operation and addressing the limitations of conventional MPPT techniques concerning tracking speed, accuracy, oscillations, and overall system efficiency. Nonetheless, it is essential to acknowledge that this approach is more intricate, and its precision is linked to the specific characteristics of the PV panel. The power obtained from the PV modules is directly affected by variable weather conditions and this negatively affects the operation of the entire system. The more we reduce fluctuations in the system, the more stable it becomes. Data collection is the first and most important step in creating an ANN-based forecast. Therefore, a voltage variation table is initially created based on the temperature and radiation changes, which are determined as input for the specified PV module. The obtained data is divided into 80% training data and 20% testing data. Various combinations of a single hidden layer between the input and output layers have been tested more than a hundred times. Since the PV voltage is a nonlinear output of temperature and irradiation, the FFBPNN type and the Levenberg-Marquardt training

function are used to address nonlinear least squares problems, based on the nonlinear activation function of tangent sigmoid transfer function. The regression graph of the proposed network is demonstrated in Figure 3.
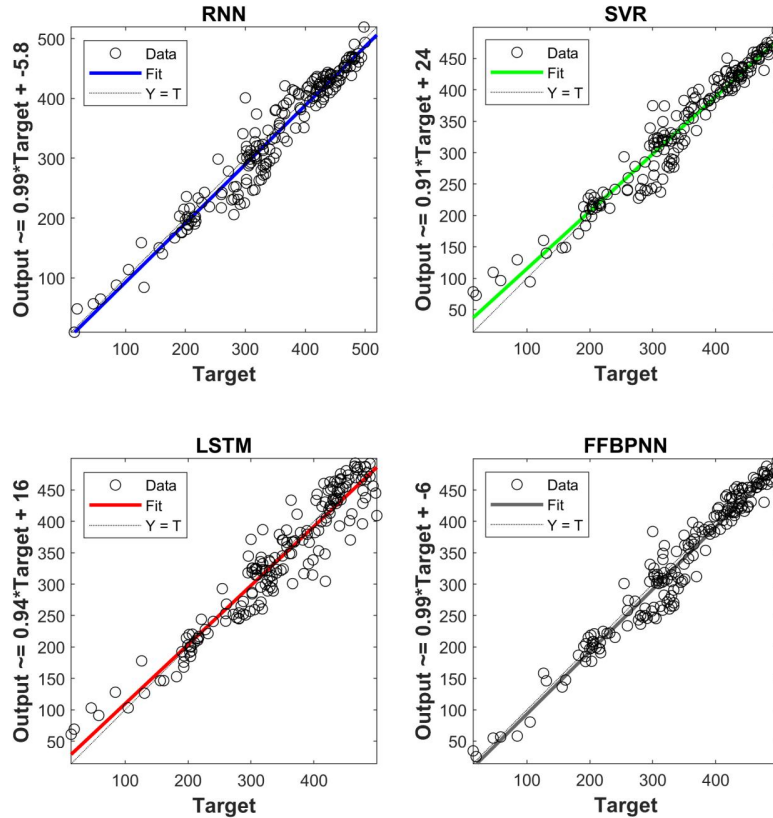

Figure 3. Regression graphs of the proposed model.

2.4. Battery energy storage system

In the BES system, the design of the battery, the design of the DC-DC bidirectional buck-boost converter, and the design of the controller for the charge and discharge processes of the battery are all essential for its creation.

2.4.1. Electrical characteristics of the battery

Together with solar energy, the BES system has begun to be used in many areas. While this provides a more ecological energy cycle for the environment, it also offers a technological solution for rural areas. Although the initial thought might be to use this hybrid system in rural areas, it is now also utilized in homes, schools, factories, etc. In the BES system, the battery design, the DC-DC bidirectional buck-boost converter design, and the PI controller design for managing the battery's charge and discharge processes are all crucial for the system's development. The lithium-ion battery selected for the battery block in MATLAB/Simulink has a nominal voltage of 420 V and a rated capacity of 24 Ah (ampere-hour). The rated capacity of the battery is specified as 10 kWh. The lower and upper limits of SOC are set at 50% and 90%, respectively. This means that the battery is designed to discharge down to 50% and charge up to 90%. The battery properties are detailed in Table 2.

2.4.2. DC-DC bidirectional buck-boost converter

The BES is connected to a DC-link with a bidirectional DC-DC buck-boost converter to adjust voltage levels during the charging and discharging processes. The topology of the DC-DC bidirectional buck-boost converter is illustrated in Figure 1. The DC-link voltage is specified as 700 V for the high voltage side of the converter, while the battery voltage is specified as 455 V for the low voltage side of the converter.

2.4.3. Design of control scheme for battery charge and discharge

The most important point after the circuit design is the correct feeding of the operating signals of the switches. The battery model utilizes the battery's SOC as the primary variable to depict the voltage behavior [37]. The charging and discharging states of the battery are examined separately.

In the charging state, the error between the voltage of the battery and the reference voltage is calculated. This difference is controlled by the PI parameters and multiplied by (–1) to obtain the reference charging current (IB_ref) for the battery at the output. Thus, both the battery voltage is controlled, and the reference charging current is determined based on the battery voltage and the produced PV power. This charging process is illustrated in Figure 4. The reference voltage is specified as 455 V, which is the voltage of the battery at 90% SOC. The maximum charging current is set at 10.43 A, with reference to the nominal discharge current of the battery in the battery block. After the reference charging current for the battery is determined, the difference between this value and the measured current of the battery is controlled by the PI parameters. The PI output is then compared with a reference signal in the (0, 1) range to generate gate signals for the charging processes. The charging process ends when the SOC of the battery reaches 90%. Since the power produced by PV varies at low radiance values and high radiance values, the power transferred to the battery and the grid constantly varies, which causes harmonic distortion to increase. In order to prevent this situation, the power transferred to the battery is provided with lower current values at low radiance values, and with higher current values at high radiance values. The power produced from PV, the power transferred to the battery, and the power transmitted to the grid are P_{PV}, P_{bt} and P_{grid}, respectively. The battery voltage and current are represented as V_{bt} and I_{bt}, respectively, and the reference current for the battery is denoted as IB_ref.

$$P_{PV} \equiv P_{bt} + P_{grid} + P_{loss} \tag{4}$$

$$P_{bt} \equiv V_{bt} * I_{bt} \tag{5}$$

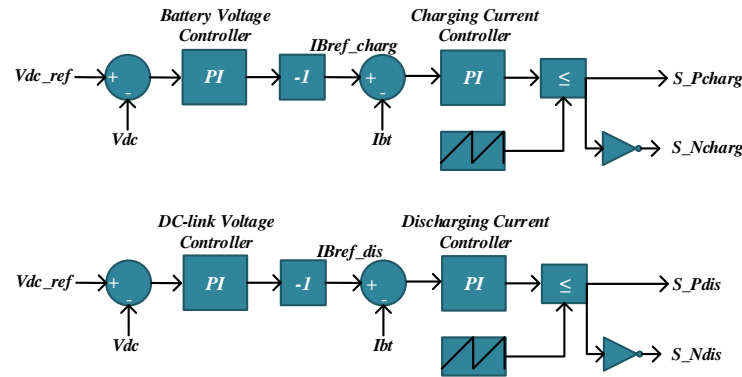$$IB\_ref \equiv \frac{P_{PV} - P_{grid}}{V_{bt}} \tag{6}$$

Figure 4. Control of the battery charging and discharging processes.

During the discharging process, the difference between the DC-link voltage and the reference voltage is fed into PI parameters to obtain the reference discharging current for the battery. This approach ensures that both the DC-link voltage is controlled and the maximum discharging current (IB_ref) of the battery is set at 10.43 A. These processes for discharging are displayed in Figure 4. After the reference discharging current for the battery is determined, the difference between this value and the measured current of the battery is controlled by the PI parameters. The PI output is then compared with a reference signal in the (0, 1) range to generate gate signals for the discharging processes. The discharging process ends when the SOC of the battery reaches 50%. In this mode, the battery transmits its power only to the grid. The discharge current of the battery is set to be high at high SOC values and lower at low SOC values.

$$P_{PV} \equiv 0 \tag{7}$$

$$P_{bt} \equiv P_{grid} \tag{8}$$

$$IB\_disc \equiv \frac{0 - P_{grid}}{V_{bt}} \equiv \frac{-P_{bt}}{V_{bt}} \tag{9}$$

2.5. Proposed power quality enhancement algorithm

The operating scenario of the system is designed to support the most effective consumption of the generated power. The consumption rates of electrical energy vary throughout the day. Different tariffs are applied based on time zones and varying levels of consumption. In Türkiye, there are three different tariff zones: the daytime period from 06:00 to 17:00, the peak period from 17:00 to 22:00, and the night period from 22.00 to 06:00. Between these periods, the highest energy consumption occurs between 17:00 and 22:00, which is the peak period. The energy consumption tariffs applied vary across these three periods. The tariff for the night period is lower than that for the day period, while the highest tariff is applied during the peak period. Therefore, it is crucial to use the produced energy effectively, that is, to manage it properly. The system operational strategy is illustrated in Figure 5.
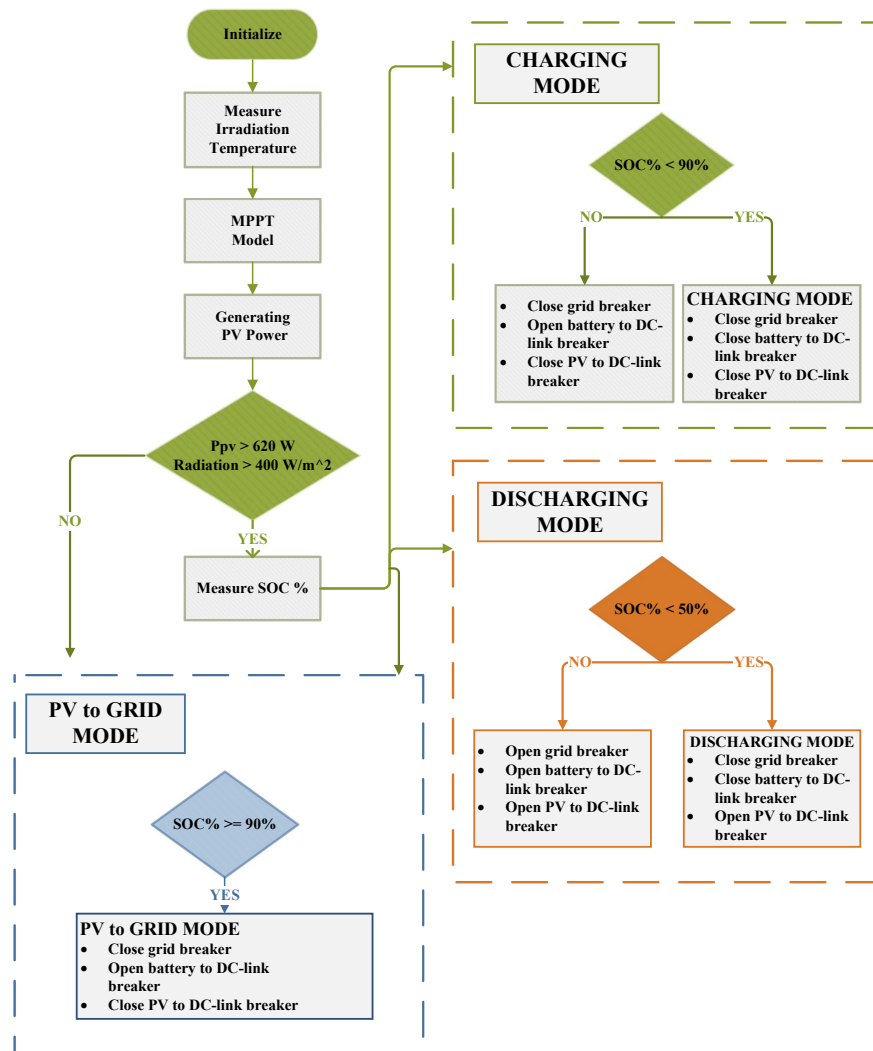
Figure 5. Operational scenario of the proposed system.

The battery in the system is charged under the following conditions: $P_{PV} > 620$ W, irradiation > 400 W/m^2, and SOC $< 90\%$. In other words, if the PV produces stable power during the daytime, if the produced power is sufficient to charge the battery, and if the battery's SOC is below 90%, then the battery will be charged until it reaches 90% SOC. This approach ensures that the battery is prepared to support the grid during peak time intervals. The irradiation must be at least 400 W/m^2 for charging the battery. This requirement arises because the battery is at 50% SOC before it starts charging. In other words, since the battery contains 5 kW of power, we must have P_{PV} greater than 5 kW to effectively charge the battery. When the function inputs meet these conditions, the function outputs enable the battery to be charged by opening the grid breaker and closing the battery breaker and DC-link breaker. In this way, the energy flow is only ensured between the PV system and the battery until it reaches 90% SOC.

The battery discharges in the system when the $P_{PV} < 620$ W and the SOC $> 50\%$. In other words, when the power generation of the PV system stops and the battery's SOC is greater than 50%, the battery discharges until it reaches 50% SOC. This process ensures that the battery is ready to support the grid during

peak times. When the function inputs meet these conditions, the function outputs close the grid breaker and the battery breaker and open the DC-link breaker, allowing the battery to discharge. Consequently, the energy flow is only provided between the battery and the grid until the battery reaches 50% SOC.

PV to grid mode is the period when all the power produced by the PV system is transmitted to the grid. For the system to operate in this mode; P_{PV} must be greater than 620 W, and the SOC must be at least 90%, or the irradiation value must be lower than 400 W/m^2. When these conditions are met, the battery breaker determined as the output will be in the open position, while the grid breaker and the DC-link breaker will be in the closed position.

3. Simulation results and discussion

The test results of the proposed system and its comparison with other MPPT methods are examined in this section. MATLAB/Simulink is used for hybrid system design. The simulation parameters of the proposed system are outlined in Table 2. The proposed system is simulated under three different cases, and the results are presented separately.

Table 2. Simulation parameters of the proposed system.

PV system		Battery properties	
Number of serially connected modules per string	12	Capacity	10 kWh
Number of parallel connected strings	2	Rated capacity	424 Ah
Voltage at MPP under STC	418.8 V	Nominal discharge current	10.43 A
Current at MPP under STC	14.9 A	Max SOC%	90%
Maximum output power under STC per array	6.24 kW	Min SOC%	50%
Total PV power	12.8 kW		
Interleaved boost converter		**Bidirectional buck-boost converter**	
Rated power per array	6.24 kw	Rated power capacity	10 kW
DC-link voltage	700 V	Switching frequency	20 kHz
Switching frequency	20 kHz	VL	455 V
Input current ripple	10%	VH	700 V
Output voltage ripple	1%	L	3.7 mH
L	6.8 mH	Duty cycle buck mode	0.64
C	0.1 mF	Duty cycle boost mode	0.36
Duty cycle	0.41		

3.1. Case 1

The proposed system is tested for three different MPPT methods based on constant radiation values such as 1000 W/m^2 and 500 W/m^2, and the THD values of the system are detailed in Table 3. Charging mode, discharging mode, PV to grid mode are presented separately for each weather condition. The graphical results of the system at 1000 W/m^2 500 W/m^2 for all operating modes are displayed in Figure 6, respectively. The SOC value is set to 50% for charging modes and 90% for PV to grid modes.

Table 3. THD results of MPPT methods.

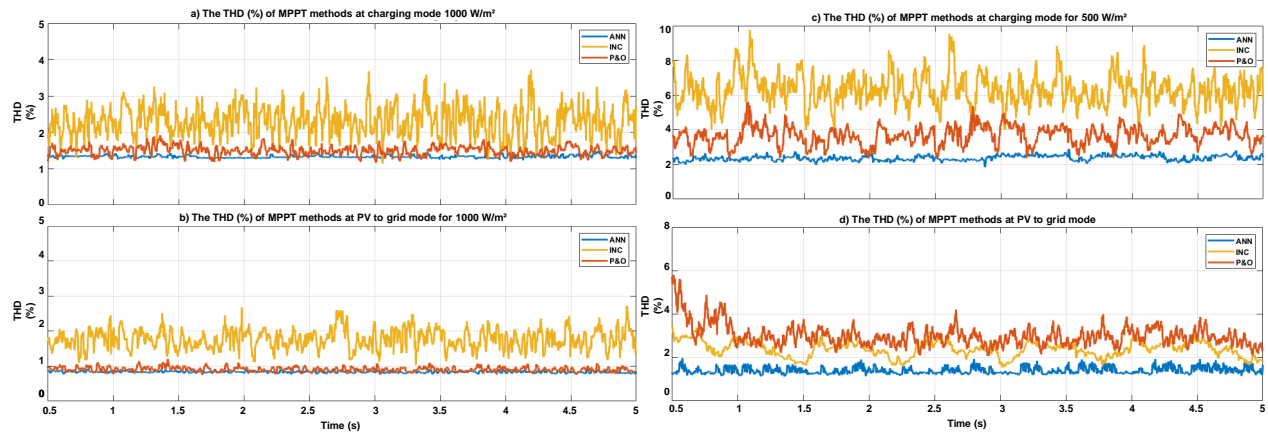| Irradiation	Operating mode	Injected method	THD%
1000 W/m^2	Charging	ANN	1.3%
1000 W/m^2	Charging	P&O	1.5%–2%
1000 W/m^2	Charging	INC	2%–4%
500 W/m^2	Charging	ANN	2%–3%
500 W/m^2	Charging	P&O	2%–4%
500 W/m^2	Charging	INC	6%–8%
1000 W/m^2	PV to grid mode	ANN	0.85%
1000 W/m^2	PV to grid mode	P&O	1%
1000 W/m^2	PV to grid mode	INC	1%–3%
500 W/m^2	PV to grid mode	ANN	1%–2%
500 W/m^2	PV to grid mode	P&O	2%–4%
500 W/m^2	PV to grid mode	INC	2%–4%

Figure 6. THD of the system: a) charging mode at 1000 W/m^2; b) PV to grid mode at 1000 W/m^2; c) charging mode at 500 W/m^2; d) PV to grid mode at 500 W/m^2.

The operational strategy based on ANN-MPPT demonstrates superior performance over traditional MPPT methods across all battery operating modes under constant radiation values, as illustrated in Figure 6. The comparison reveals that traditional MPPT methods exhibit more oscillations compared to ANN-MPPT. The results highlight its stability and capability to achieve notably lower THD values. This feature is crucial for enhancing power quality and optimizing efficiency in power systems.

3.2. Case 2

The proposed system is evaluated based on the radiation curve in Figure 7. The initial battery SOC value is set to 51%. The proposed system is simulated for three different MPPT methods under the given radiation value. The graphs in Figures 8 and 9 depict fluctuations in the DC-link voltage, THD variations of the system, and changes in battery SOC, current, and voltage.
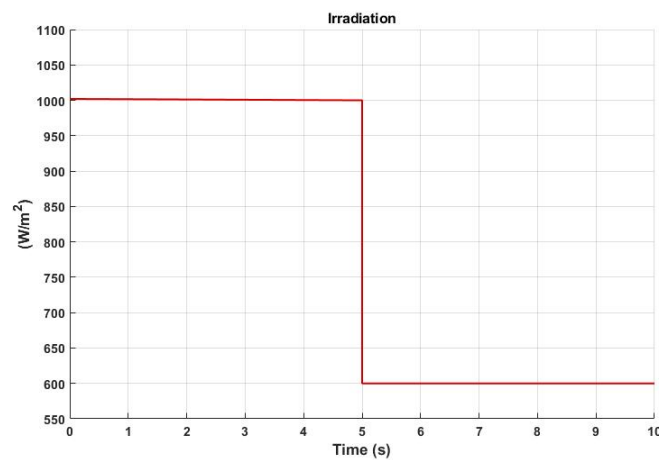

Figure 7. Radiation curve for case 2.

According to the operational strategy, when the proposed system is tested with the irradiation value shown in Figure 7, the system operates in charging mode at 1000 W/m^2, and the battery is charged at 10 A due to the high irradiation value. In the graphs, the response of the MPPT methods can be observed when the irradiation value suddenly drops to 600 W/m^2. At 600 W/m^2, according to the operational strategy, the battery continues to charge because the SOC is below 90%. However, as the irradiation value decreases, the generated PV power also decreases, resulting in the battery being charged at 5 A. Examination of the battery SOC, current, and voltage graphs confirms that the operational strategy is functioning correctly.
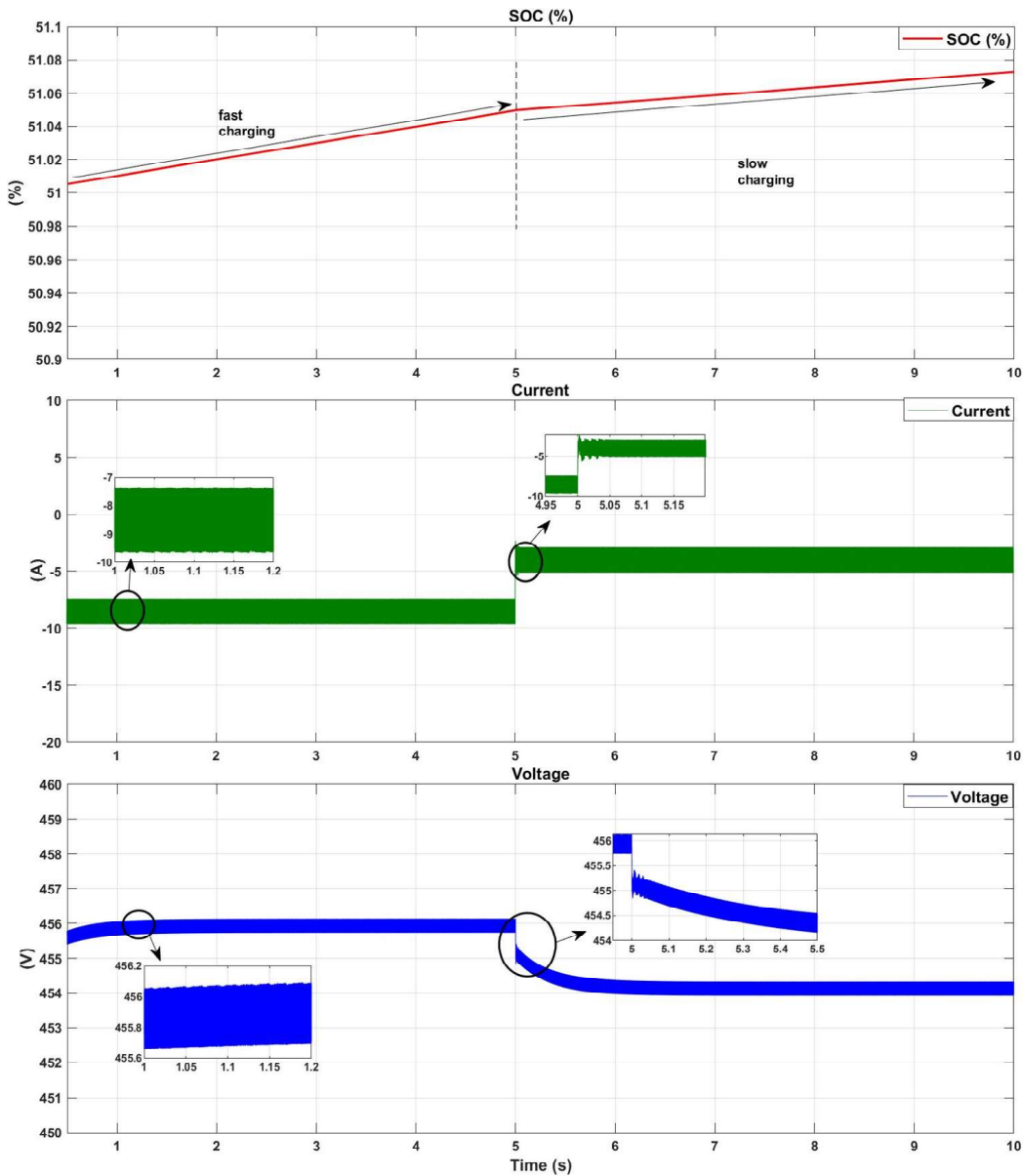

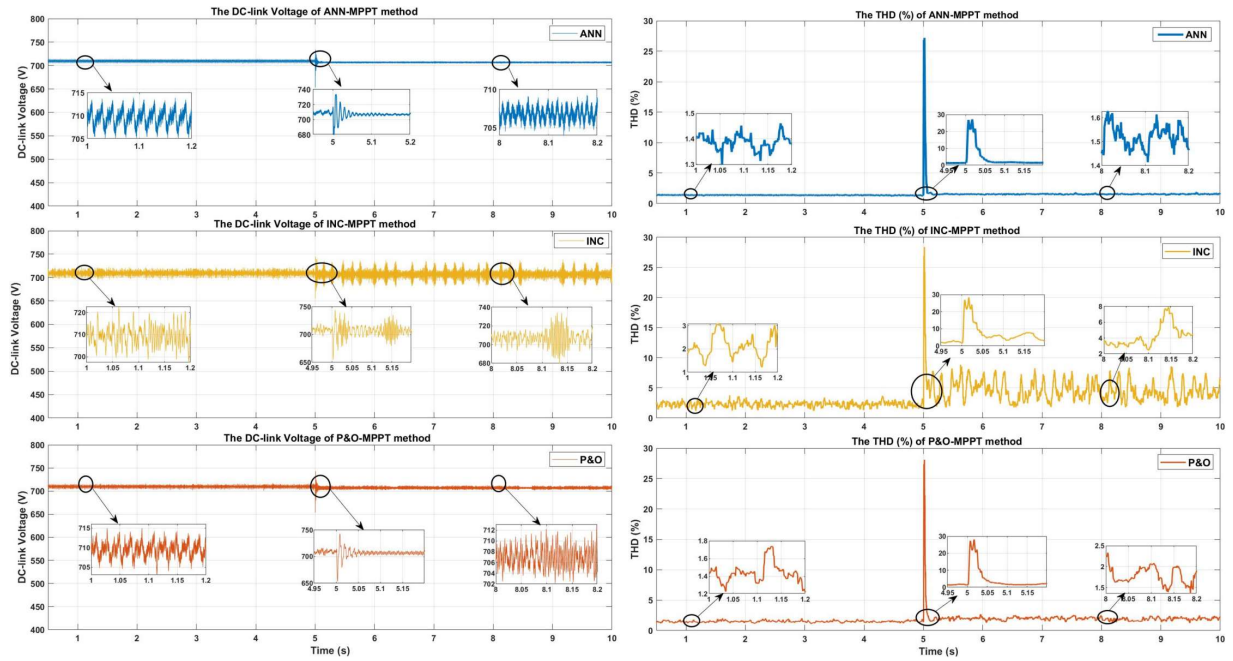**Figure 8.** SOC, current, and voltage of the battery for case 2.

Figure 9. DC-link voltage and THD of the system for MPPT methods for case 2.

When analyzing the DC-link voltages depicted in Figure 9, both ANN-MPPT and P&O-MPPT demonstrate comparable voltage levels under 1000 W/m^2, while INC-MPPT exhibits pronounced oscillations. Upon sudden radiation changes, it becomes clear that the DC-link voltage of the ANN-MPPT method maintains closer alignment with the reference value and exhibits less deviation compared to other methods. At 600 W/m^2, the system utilizing ANN-MPPT demonstrates enhanced stability in both DC-link voltage behavior and THD metrics.

3.3. Case 3

The operation of the system is also investigated depending on the radiation curve of a day created from real meteorological data of Tarsus/Mersin. The graph in Figure 10 displays the variation of solar radiation throughout the day. With this created variable solar radiation, the system scenario in Figure 5 is tested within the scope of energy management and the results of the MPPT methods are compared.
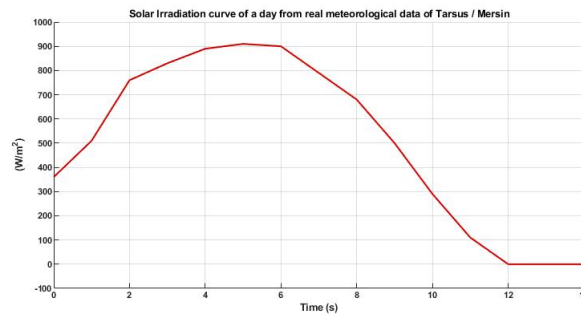

Figure 10. Solar radiation curve of a determined day.

The simulation time is 14 s. Since it takes a long time to charge the battery in the simulation environment, every second spent in the simulation is considered an hour. It is thought that our PV system starts to generate power at 05:00 AM and simulation results are shown until 19:00. In the simulation, the radiation curve's initial value at 0 corresponds to the actual daily irradiation value at 05:00 AM, indicating that the PV system starts to generate power at a specific time. The initial battery SOC value is set at 51% for this case. The graphs in Figures 11 and 12 depict fluctuations in the DC-link voltage, THD variations of the system, and changes in battery SOC, current, and voltage. According to the scenario in Figure 5, when the system starts operating with the radiation shown in Figure 10; it works in discharging mode until the radiation reaches 400 W/m^2 since the SOC is less than 90%. Once the radiance is greater than 400 W/m^2, the power generated from the PV is transmitted to both the battery and the grid, and the battery starts charging. In this case, slow charging occurs because the battery is charged with low current due to the low radiation; however, if the radiance exceeds 750 W/m^2, the battery charging current increases, and fast charging occurs. The battery stops charging and begins discharging once the irradiation drops below 400 W/m^2, provided that the SOC is greater than 50%. In summary, for this radiation graph, the system operates sequentially in discharge, slow charge, fast charge, slow charge, and discharge modes according to the operational strategy. The battery SOC graph in Figure 11 clearly demonstrates the effective implementation of the operational strategy.
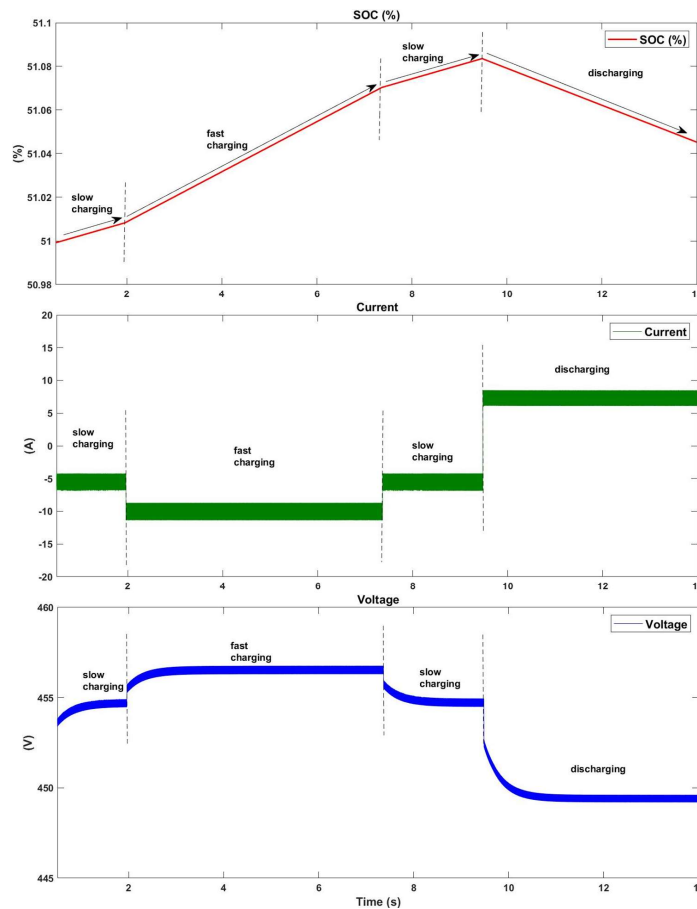

Figure 11. SOC, voltage, and current of the battery for case 3.

Examination of the DC bus voltage graphs in Figure 12 reveals that the ANN-MPPT method demonstrates smoother voltage fluctuations compared to other MPPT methods, especially noticeable under low radiation conditions. Given the varying nature of solar radiation levels throughout the day, which are not consistently at their maximum, this feature significantly enhances the system's stability, efficiency, and overall power quality. When the THD graphs in Figure 12 are analyzed, it is seen that the THD of the ANN-based model responds more quickly to variable weather conditions and settles more quickly with less oscillations. During the initial 2 s of slow charging mode, the THD of the ANN-MPPT model remains below 3%, whereas the INC-MPPT and P&O-MPPT methods struggle to achieve stability. During the battery's fast charging mode, the THD of the ANN-MPPT model stays below 2%, whereas the INC-MPPT and P&O-MPPT methods exhibit THD levels below 3% but with noticeable oscillations. It is observed that the sudden change between charging modes between 7 and 8 s greatly affects the system stability of INC-MPPT and P&O-MPPT methods, and the oscillation increases until the switch to discharge mode. Throughout this interval, the THD value of the ANN-MPPT method generally remains below 3%, ensuring system stability. During the battery's discharge mode, the THD value of the ANN-MPPT model shows fewer oscillations, staying below 3%, whereas the other methods exhibit more oscillations with THD values below 4%.
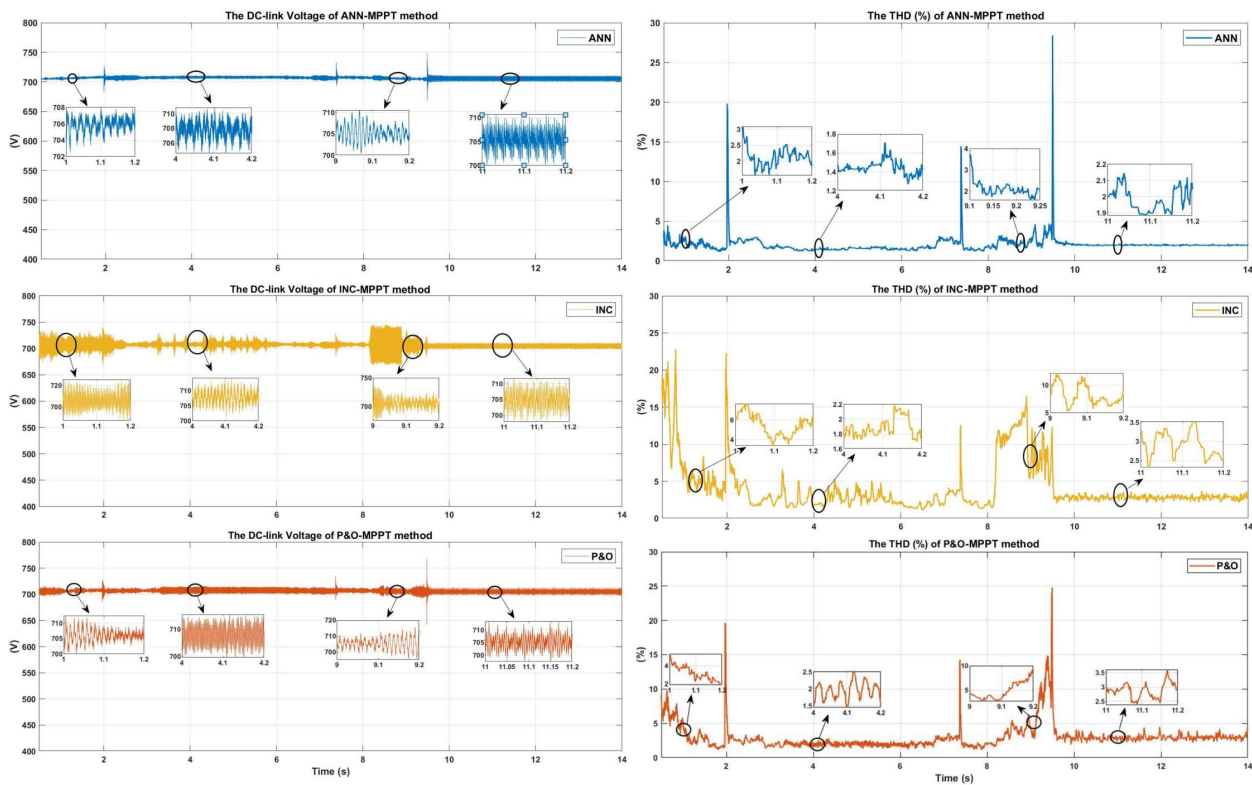

Figure 12. THD of the system based on MPPT methods for case 3.

4. Conclusion

In conclusion, this study successfully models and tests a hybrid PVBES system in the Matlab/Simulink environment, integrating a 12-kW PV plant with a 10-kWh capacity BES. The system is evaluated under three different cases: constant radiation, rapid fluctuating radiation, and real-day solar radiation data from Tarsus/Mersin, employing an operational strategy based on ANN-MPPT, P&O-MPPT, and INC-MPPT methods. Under constant irradiance conditions, the ANN-MPPT method demonstrated significant system stability, maintaining a THD below 3% during both PV to grid mode and charging mode at 1000 W/m² and 500 W/m², respectively. This performance underscores the method's ability to handle steady-state scenarios effectively, ensuring optimal power quality and efficiency. In the case of rapidly changing irradiance, the DC-link voltage stability exhibited by the ANN-MPPT method surpasses that of other methods in both fast and slow charge modes, ensuring the system maintains a THD of less than 3%, thereby enhancing the overall power quality. When the hybrid system was tested using measured solar radiation data from Tarsus/Mersin, the ANN-MPPT method again outperformed the INC-MPPT and P&O-MPPT methods. It exhibited lower system THD and greater stability during abrupt changes in irradiance. Specifically, the DC-link voltage with ANN-MPPT maintained a narrower fluctuation range of 700–710 V with a deviation of 1.4%, compared to the wider ranges observed with INC-MPPT and P&O-MPPT (700–720 V) with a deviation of 2.8%. This consistency is critical for maintaining system efficiency and reliability in real-world conditions where solar irradiance is highly variable. The simulation results clearly indicate that the ANN-based MPPT operational strategy significantly enhances system stability, improves power quality, and reduces THD across various solar irradiance conditions. The method's ability to quickly converge to the maximum power point with minimal oscillations further validates its superiority over traditional MPPT methods. These findings highlight the potential of the ANN-MPPT method in practical hybrid PV-BES systems, offering a more reliable and efficient solution for renewable energy integration. However, the method may face regulatory, technical, and operational challenges, including grid stability requirements and implementation complexity.

References

[1] Chauhan S, Singh B. Control of solar PV-integrated battery energy storage system for rural area application. IET Renewable Power Generation 2021; 15 (5): 1030-1045. https://doi.org/10.1049/rpg2.12086

[2] Liang X, Andalib-Bin-Karim C. Harmonic mitigation through advanced control methods for grid-connected renewable energy sources. In: 2017 IEEE Industry Applications Society Annual Meeting; Cincinati, OH, USA; 2017. pp. 1-12. https://doi.org/10.1109/IAS.2017.8101861

[3] Iqbal MM, Islam K. Design and simulation of a PV system with battery storage using bidirectional DC-DC converter using Matlab Simulink. International Journal of Scientific & Technology Research 2017; 6 (07): 403-410.

[4] Bollipo RB, Mikkili S, Bonthagorla PK. Hybrid, optimal, intelligent and classical PV MPPT techniques: a review. CSEE Journal of Power and Energy Systems 2021; 7 (1): 9-33. https://doi.org/10.17775/CSEEJPES.2019.02720

[5] Narayanan V, Kewat S, Singh B. Solar PV-BES based microgrid system with multifunctional VSC. IEEE Transactions on Industry Applications 2020; 56 (3): 2957-2967. https://doi.org/10.1109/TIA.2020.2979151

[6] Hannan MA, Wali SB, Ker PJ, Abd Rahman MS, Mansor M et al. Battery energy-storage system: a review of technologies, optimization objectives, constraints, approaches, and outstanding issues. Journal of Energy Storage 2021; 42: 103023. https://doi.org/10.1016/j.est.2021.103023

[7] Alexander SA. Development of solar photovoltaic inverter with reduced harmonic distortions suitable for Indian subcontinent. Renewable and Sustainable Energy Reviews 2016; 56: 694-704. https://doi.org/10.1016/j.rser.2015.11.092

[8] Çelik Ö, Teke A. A hybrid MPPT method for grid connected photovoltaic systems under rapidly changing atmospheric conditions. Electric Power Systems Research 2017; 152: 194-210. https://doi.org/10.1016/j.epsr.2017.07.011

[9] Senapati MK, Pradhan C, Nayak PK, Samantaray SR. Lagrange interpolating polynomial–based deloading control scheme for variable speed wind turbines. International Transactions on Electrical Energy Systems 2019; 29 (5): 1-17. https://doi.org/10.1002/2050-7038.2824

[10] Senapati MK, Pradhan C, Samantaray SR, Nayak PK. Improved power management control strategy for renewable energy-based DC micro-grid with energy storage integration. IET Generation, Transmission & Distribution 2019; 13 (6): 838-849. https://doi.org/10.1049/iet-gtd.2018.5019

[11] Priyadarshi N, Padmanaban S, Bhaskar MS, Blaabjerg F, Sharma A. Fuzzy SVPWM-based inverter control realisation of grid integrated photovoltaic-wind system with fuzzy particle swarm optimisation maximum power point tracking algorithm for a grid-connected PV/wind power generation system: hardware implementation. IET Electric Power Applications 2018; 12 (7): 962-971. https://doi.org/10.1049/iet-epa.2017.0804

[12] Priyadarshi N, Padmanaban S, Kiran Maroti P, Sharma A. An extensive practical investigation of FPSO-based MPPT for grid integrated PV system under variable operating conditions with anti-islanding protection. IEEE Systems Journal 2019; 13 (2): 1861-1871. https://doi.org/10.1109/JSYST.2018.2817584

[13] Senapati MK, Pradhan C, Nayak PK, Padmanaban S, Gjengedal T. Modified demagnetisation control strategy for low-voltage ride-through enhancement in DFIG-based wind systems. IET Renewable Power Generation 2020; 14 (17): 3487-3499. https://doi.org/10.1049/iet-rpg.2019.1128

[14] Reveles-Miranda M, Flota-Bañuelos M, Chan-Puc F, Ramirez-Rivera V, Pacheco-Catalán D. A hybrid control technique for harmonic elimination, power factor correction, and night operation of a grid-connected PV inverter. IEEE Journal of Photovoltaics 2020; 10 (2): 664-675. https://doi.org/10.1109/JPHOTOV.2019.2961600

[15] Sorte PK, Panda KP, Panda G. Current reference control based MPPT and investigation of power management algorithm for grid-tied solar PV-battery system. IEEE Systems Journal 2022; 16 (1): 1-11. https://doi.org/10.1109/JSYST.2021.3052959

[16] Jiang M, Ghahremani M, Dadfar S, Chi H, Abdallah YN et al. A novel combinatorial hybrid SFL–PS algorithm based neural network with perturb and observe for the MPPT controller of a hybrid PV-storage system. Control Engineering Practice 2021; 114: 104880. https://doi.org/10.1016/j.conengprac.2021.104880

[17] Priyadarshi N, Padmanaban S, Bhaskar MS, Khan B. An experimental performance verification of continuous mixed P-norm based adaptive asymmetrical fuzzy logic controller for single stage photovoltaic grid integration. IET Renewable Power Generation 2022; 1-11. https://doi.org/10.1049/rpg2.12410

[18] Priyadarshi N, Sanjeevikumar P, Bhaskar MS, Azam F, Taha IBM et al. An adaptive TS-fuzzy model based RBF neural network learning for grid integrated photovoltaic applications. IET Renewable Power Generation 2022; 16 (14): 3149-3160. https://doi.org/10.1049/rpg2.12505

[19] Priyadarshi N, Bhaskar MS, Sanjeevikumar P, Azam F, Khan B. High-power DC-DC converter with proposed HSFNA MPPT for photovoltaic based ultra-fast charging system of electric vehicles. IET Renewable Power Generation 2022; 1-13. https://doi.org/10.1049/rpg2.12513

[20] Thangella R, Yarlagadda SR, Sanam J. Optimal power quality improvement in a hybrid fuzzy-sliding mode MPPT control-based solar PV and BESS with UPQC. International Journal of Dynamics and Control 2023; 11 (4): 1823-1843. https://doi.org/10.1007/s40435-022-01095-0

[21] El Mezdi K, El Magri A, Watil A, El Myasse I, Bahatti L et al. Nonlinear control design and stability analysis of hybrid grid-connected photovoltaic-battery energy storage system with ANN-MPPT method. Journal of Energy Storage 2023; 72 (Part E): 108747. https://doi.org/10.1016/j.est.2023.108747

[22] Gali V, Jamwal PK, Gupta N, Kumar A. Multimode control strategy to improve the power quality and autonomy of PV-Wind-BESS based microgrid using harmonic frequency adaptive observer filter. Electric Power Systems Research 2023; 225: 109786. https://doi.org/10.1016/j.epsr.2023.109786

[23] Morey M, Gupta N, Garg MM, Kumar A, Gali V. Experimental investigation of ANFIS-PSO MPPT control with enriched voltage gain DC–DC converter for grid-tied PV applications. Electrical Engineering 2024. https://doi.org/10.1007/s00202-023-02192-9

[24] Çelik Ö. Data-driven MPPT techniques for optimizing vehicular fuel cell performance in hybrid DC microgrid. International Journal of Hydrogen Energy 2024; 79: 715-727. https://doi.org/10.1016/j.ijhydene.2024.07.033

[25] Bozkurt H. Optimal design of a hybrid PV-battery system for on-grid applications. MSc Thesis, Çukurova University, Adana, Türkiye, 2022.

[26] Alharbi BM, Alhomim MA, McCann RA. An efficient high voltage gain using two-stage cascaded interleaved boost converter for solar PV system with MPPT technique. In: 2020 IEEE Power & Energy Society Innovative Smart Grid Technologies Conference; Washington, DC, USA; 2020. pp. 49-52. https://doi.org/10.1109/ISGT45199.2020.9087720

[27] Zongo OA. Comparing the performances of MPPT techniques for DC-DC boost converter in a PV system. Walailak Journal of Science and Technology 2021; 18 (2): 1-15. https://doi.org/10.48048/wjst.2021.6500

[28] Sher HA, Murtaza AF, Noman A, Addoweesh KE, Al-Haddad K et al. A new sensorless hybrid MPPT algorithm based on fractional short-circuit current measurement and P&O MPPT. IEEE Transactions on Sustainable Energy 2015; 6 (4): 1426-1434. https://doi.org/10.1109/TSTE.2015.2438781

[29] Basha CHH, Rani C. Different conventional and soft computing MPPT techniques for solar PV systems with high step-up boost converters: a comprehensive analysis. Energies 2020; 13 (2): 371. https://doi.org/10.3390/en13020371

[30] Bhattacharyya S, Kumar P DS, Samanta S, Mishra S. Steady output and fast tracking MPPT (SOFT-MPPT) for P&O and InC algorithms. IEEE Transactions on Sustainable Energy 2021; 12 (1): 293-302. https://doi.org/10.1109/TSTE.2020.2991768

[31] Guerra MIS, Ugulino de Araújo FM, Dhimish M, Vieira RG. Assessing maximum power point tracking intelligent techniques on a pv system with a buck–boost converter. Energies 2021; 14 (22): 7453. https://doi.org/10.3390/en14227453

[32] Ibnelouad A, El Kari A, Ayad H, Mjahed M. Multilayer artificial approach for estimating optimal solar PV system power using the MPPT technique. Studies in Informatics and Control 2021; 30 (4): 109-120. https://doi.org/10.24846/V30I4Y202110

[33] Talbi M, Mensia N, Ezzaouia H. Modeling of a PV panel and application of maximum power point tracking command based on ANN. The International Arab Journal of Information Technology 2021; 18 (4): 568-577. https://doi.org/10.34028/18/4/9

[34] Bozkurt H, Macit R, Çelik Ö, Teke A. Evaluation of artificial neural network methods to forecast short-term solar power generation: A case study in Eastern Mediterranean Region. Turkish Journal of Electrical Engineering & Computer Sciences 2022; 30 (6): 2013-2030. https://doi.org/10.55730/1300-0632.3921

[35] Abiodun OI, Jantan A, Omolara AE, Dada KV, Mohamed NAE et al. State-of-the-art in artificial neural network applications: a survey. Heliyon 2018; 4 (11): e00938. https://doi.org/10.1016/j.heliyon.2018.e00938

[36] Yap KY, Sarimuthu CR, Lim JMY. Artificial intelligence based MPPT techniques for solar power system: a review. Journal of Modern Power Systems and Clean Energy 2020; 8 (6): 1043–1059. https://doi.org/10.35833/MPCE.2020.000159

[37] Tremblay O, Dessaint LA. Experimental validation of a battery dynamic model for EV applications. World Electric Vehicle Journal 2009; 3 (2): 289-298. https://doi.org/10.3390/wevj3020289